2013 IREP Symposium-Bulk Power System Dynamics and Control -IX (IREP), August 25-30, 2013, Rethymnon, Greece

Applications of Synchrophasor Data to Power System State Estimation and Control

Scott G. Ghiocel
Rensselaer Polytechnic Institute
Troy, NY, USA

Daniel Dotta
Federal Institute of Santa Catarina
Florianopolis, SC, Brazil

Joe H. Chow
Rensselaer Polytechnic Institute
Troy, NY, USA

Abstract

The installation of phasor measurement units (PMUs) around the world enables wide-area monitoring and control applications. To incorporate PMU data in grid operations, system operators must understand, validate, and correct phasor measurements before using them in higher-level applications. In this paper, we first discuss the phasor measurement process that takes place inside a PMU, then we present a phasor state estimator to correlate and validate PMU data across a network, and finally we discuss a two-level interarea mode damping controller using remote phasor measurements.

Introduction

Today, there are several Wide-Area Measurement Systems (WAMS) operating around the world. Despite the different development stages and applications found in different countries their Independent System Operators (ISOs) recognize the importance of wide-area monitoring and control. The US power grid is currently installing close to 1,000 new phasor measurement units (PMUs) as part of the US DOE Smart Grid Investment Grant (SGIG) activity. It is envisioned that the high-sampling-rate data captured by PMUs distributed across a power grid can be used to improve the visibility across control areas and enhance system reliability.

The paper will be divided in three main parts. In the first part, the phasor measurement estimation process is discussed. The understanding of the phenomena involved in the phasor measurement process is necessary for correct phasor data analysis as well as for design of advanced control and protection schemes. This process knowledge also allows the identification of potential sources of errors helping the incorporation of phasor measurement in the state estimator process.

In the second part, a phasor state estimator (PSE) capable of correcting phase biases and scaling factors will be described. The application of this phasor state estimator to the central New York power system will be illustrated. With sufficient redundancy, the PMUs on six substations allow signal calibration and voltage phasor calculation on seven neighboring buses. As a result, the impact of internal and external disturbances on the major power transfer paths in central New York can be studied in greater details. Currently we are planning on expanding the coverage of this phasor state estimator to additional regions in New York.

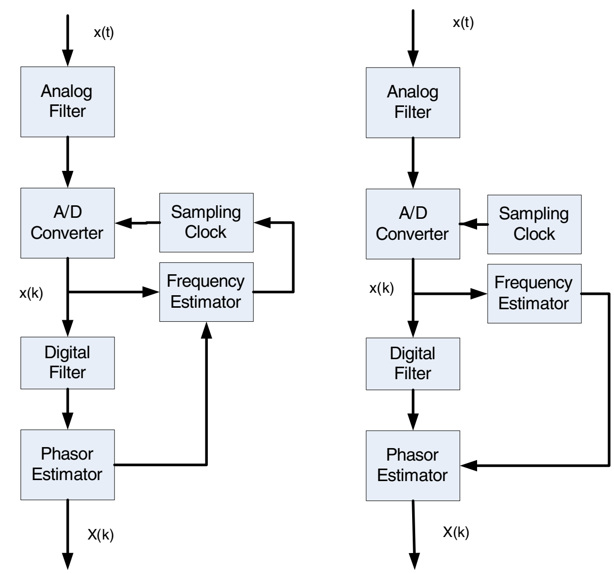

Fig. 1. Basic Phasor estimation architectures [1]

In the third part, interarea mode damping using remote PMU signals will be presented. Here the emphasis is on two-level control schema design. For a damping controller to be effective, it has to provide appropriate phase compensation, mostly of the lead type. The two-level control shown a better performance when compared to the decentralized control schema.

Phasor Measurements Architectures

Figure 1 illustrates the two basic PMU architectures [1]. The basic block diagrams for the two schemes are similar and can be divided into:

- Sampling and filtering;
- Frequency and Phasor (Discrete Fourier Transform - DFT) estimators.

The main difference between the architectures is in the way the signal is sampled:

- A uniform (fixed) sampling rate;
- A non-uniform (variable) sampling rate.

The first architecture was the first being used because uniform sampling simplifies the data acquisition process and the signal-processing analysis. Most of PMU algorithm development activities are based on exploring and improving uniform sampling methodologies [2], [3], [4], [5], [6] and [7]. As a result, this paper will focus on the uniform sampling rate approach.

There are some non-uniform sampling methodologies available from the literature. An early result is available in [8], followed by a few papers [6]; and some US patents [9] [10]. The main technical issue is to relate the time-tag given by the GPS clock to the sampling clock generated by the local power system frequency measurement.

Uniform Sampling Phasor Measurement Processing

The uniform sampling phasor measurement process is divided in three main parts: phasor estimation using (recursive or non-recursive) discrete Fourier Transform (DFT), frequency estimation, and post-processing (using calibration factors and filtering), as shown in Figure 2. Under off-nominal frequency operation, the post-processing layer is necessary to correct the effects caused by the leakage phenomenon. The leakage phenomenon results from the truncation of sampled data outside the data window. Consequently, the estimated phasor is attenuated by two complex gains, P_n and Q_n.

$$X^{est} = PX^{true} + Q(X^{true})^* \tag{1}$$

where,

$$P_n = \left\{ \frac{\sin \frac{N(\omega-\omega_0)\Delta t}{2}}{N \sin \frac{(\omega-\omega_0)\Delta t}{2}} \right\} e^{j(N-1)\frac{(\omega-\omega_0)\Delta t}{2}} \tag{2}$$

$$Q_n = \left\{ \frac{\sin \frac{N(\omega+\omega_0)\Delta t}{2}}{N \sin \frac{(\omega+\omega_0)\Delta t}{2}} \right\} e^{-j(N-1)\frac{(\omega+\omega_0)\Delta t}{2}} \tag{3}$$

From Equation (2), the effects of the complex gain P_n (shown in Figure 2) can be readily computed from the sampling window size (N), the frequency deviation ($\Delta\omega$) and the sampling period ($\triangle t$) [2]. The magnitude of P_n is an attenuation factor, and the phase angle of P_n is a constant offset in the measured phase angles. As the window size (N) and sampling period ($\triangle t$) are fixed, P_n can be readily estimated for a frequency range and stored in a table (Block 1 in Figure 2). In real-time, frequency deviation estimation is necessary to compute the correct P_n value.

The complex gain Q_n introduces a magnitude and phase angle variations at frequency $2\omega_0 + \Delta\omega \simeq 2\omega_0$ (approximately) in the estimated single-phase phasor. The second harmonic ($2\omega_0$) oscillation is shown in Figure 3 (blue curve). In contrast to a static offset, this oscillation is not easily removed. A conventional way to minimize its influence is to use a three-point-average filter (Block 2 in Figure 2) [2], which can reduce the harmonic components by more than 50%. Other filtering techniques are presented in [11]. It should be noted that a similar behavior shows up in positive-sequence estimation under unbalance power system networks.

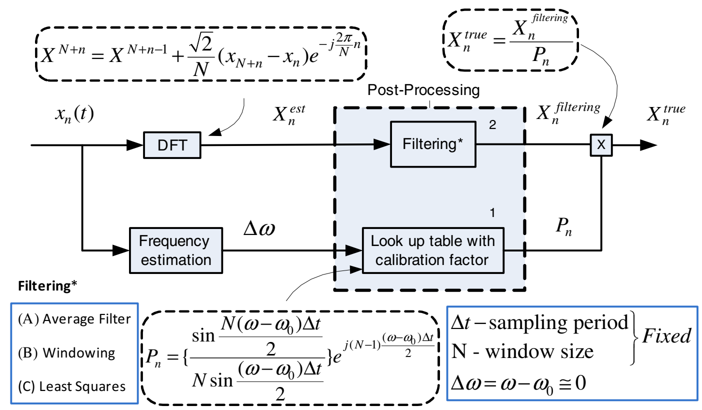

Fig. 2. Phasor processing algorithm for uniform sampling [3]

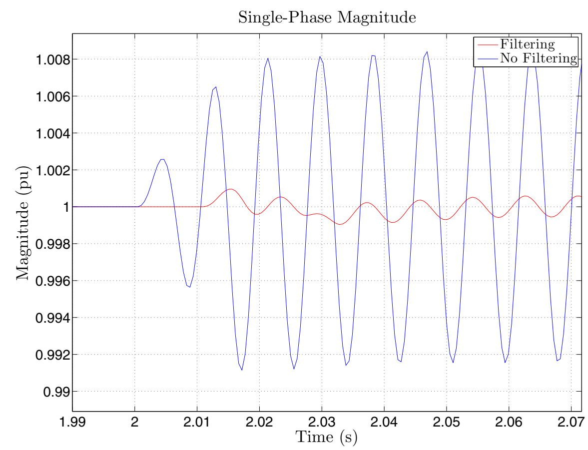

Fig. 3. Single-Phase Magnitude Estimation Performance

Frequency Estimation In normal power system operation, the power system frequency is never steady. This deviation can be small, when related to generation load mismatch, or large, during loss of generation disturbances. Thus, the frequency estimation methodology plays a key role in the phasor computation process. An interesting overview of the power system frequency concept is found in [1].

Several frequency measurement methodologies can be found in the literature [12]–[18]. The main available methods are: Zero Crossing [13], Least Error Squares [19], Kalman filters [20], Demodulation [14], [18] and Phasor-Based [13], [16], [17].

The Phasor-Based method is generally used into commercial PMUs. This method provides satisfactory performance under large frequency variation and noisy environment.

Phasor State Estimation

In this section, we describe a phasor state estimator (PSE) for improving the quality of PMU data for use in higher-level applications. We extend the PSE concept in [21] to include tap position estimation, current channel scaling, and line parameter estimation. We apply the technique to PMU data

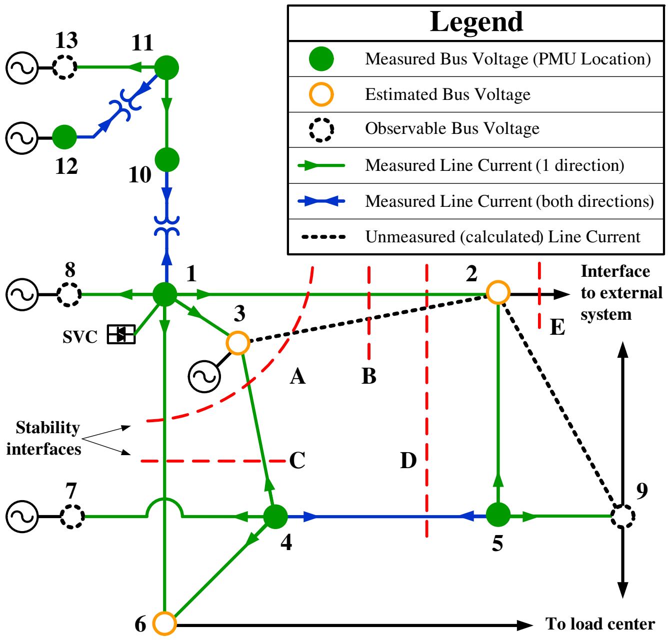

Fig. 4. Observable sub-network of a Central NY with several power transfer interfaces

from the high-voltage Central NY subnetwork (Fig. 4), which has greater redundancy and wider geographical coverage than the small system in [21]. In addition, the flows on five major power transfer interfaces (labeled as A to E) can be computed, showing the dynamic impact of various disturbances.

For the NY system in Fig. 4, voltage phasor measurements are available on five buses (Buses 1, 4, 5, 10, 11, and 12), as well as all line current phasors from those buses. The redundancy of phasor data in the NY system allows for error corrections of angle bias and current magnitude scaling, and the data can be employed to estimate transformer tap ratios and transmission line parameters. This allows for more precise and consistent PSE solutions, which will be shown in the next two sections.

Phasor Measurement Error

Measurement noise is typically assumed to be independent Gaussian white noise [22]. In our approach, we include corrections for three specific types of error in the PMU data: inaccurate line parameters, instrumentation bias, and PMU algorithm discrepancies. We correct inaccurate line parameters or transformer tap ratios by estimating the parameter in question simultaneously with the voltage phasor states. To improve the PSE solution, selected current measurements are adjusted using a correction factor. Phase angle measurements are sensitive to inaccurate synchronization, which can cause an angle bias. For each multi-channel PMU, we introduce one angle bias correction factor, as described in [21].

Least-Squares Estimation

To estimate the network state based on a set of phasor measurements ($\mathbb{M}$), we solve a weighted least-squares (WLS) problem

$$\min_{x,\alpha} \quad \sum W_i e_i^2 \tag{4}$$

$$\text{subj to} \quad e_i = z_i - h_i(x;\alpha), \quad \forall\ i \in \mathbb{M} \tag{5}$$

where x is the state vector and α is a vector containing augmented variables such as angle biases, current magnitude scaling factors, and line parameters to be estimated. The ith phasor measurement z_i is related to the states x via the function $h_i(x)$. We minimize the residual (e_i) between a measured value and the state of the underlying system model. A weight W_i is applied in the objective function to account for the variance of each measurement and we solve the optimization using the Gauss-Newton iterative method [23]. The results provide the estimated state of the system, i.e., voltage phasors at all buses and estimates for the augmented variables. To set up the WLS problem, we develop the measurement model for voltage and current phasor measurements and form the residual equations $e_i = z_i - h_i(x;\alpha)$.

PSE Measurement Equations

For each voltage phasor measurement on Bus i, we have two measurement equations (magnitude and phase). We include an angle bias term in the angle equation to account for the phase angle error introduced by shared timing circuitry and phasor processing algorithms of a multi-channel PMU. We express the voltage phasor in polar form instead of rectangular coordinates, such that the angle bias term only appears in one of the equations. When phase angle bias is included, the measurement equations are

$$e_{V_i} = V_i - V_i^{\text{meas}} \tag{6}$$

$$e_{\theta_i} = \theta_i - \theta_i^{\text{meas}} - \phi_m \tag{7}$$

where V_i^{meas} and θ_i^{meas} are the measured synchrophasor quantities and V_i and θ_i are the voltage magnitude and angle states, respectively. The angle bias term ϕ_m is associated with the m-th PMU.

For the current phasors, we set each measurement equal to the current phasor calculated using the π-model of the line and the voltage states. As in the case of the voltage phasors, we express the currents in polar form and include an angle bias term in the angle equation.

We can include a current scaling correction factor to account for poor calibration and/or nonlinearity of the CTs. If the current magnitude measurement is to be corrected, its scaling correction factor c_{ik} appears only in the magnitude equation (8). If no scaling correction is applied to a particular line current measurement then its corresponding c_{ik} term is set to zero.

On a line connecting Buses i and k, a current phasor measurement from PMU m yields error equations given by

$$e_{I_{ik}} = (1 + c_{ik})I_{ik} - I_{ik}^{\text{meas}} \tag{8}$$

$$e_{\delta_{ik}} = \delta_{ik} - \delta_{ik}^{\text{meas}} - \phi_m \tag{9}$$

where I_{ik}^{meas} and $\delta_{ik}^{\text{meas}}$ are the magnitude and phase of the current phasor measurement, respectively. The direction of the current is taken to be from Bus i to Bus k. I_{ik} and δ_{ik} are the magnitude and phase values of the calculated current phasor,

$$I_{ik} = |\tilde{I}_{ik}| = \sqrt{\left(I_{ik}^{\text{Re}}\right)^2 + \left(I_{ik}^{\text{Im}}\right)^2} \tag{10}$$

$$\delta_{ik} = \arg\left(\tilde{I}_{ik}\right) = \arctan\left(\frac{I_{ik}^{\text{Re}}}{I_{ik}^{\text{Im}}}\right) \tag{11}$$

where I_{ik}^{Re} and I_{ik}^{Im} are the real and imaginary parts of the estimated current phasor,

$$\begin{aligned} I_{ik}^{\text{Re}} = {} & (V_i \cos\theta_i - V_k \cos\theta_k)\left(\frac{R}{R^2 + X^2}\right) \\ & + (V_i \sin\theta_i - V_k \sin\theta_k)\left(\frac{X}{R^2 + X^2}\right) - \frac{1}{2}B\left(V_i \sin\theta_i\right) \end{aligned} \tag{12}$$

$$\begin{aligned} I_{ik}^{\text{Im}} = {} & (V_i \sin\theta_i - V_k \sin\theta_k)\left(\frac{R}{R^2 + X^2}\right) \\ & - (V_i \cos\theta_i - V_k \cos\theta_k)\left(\frac{X}{R^2 + X^2}\right) + \frac{1}{2}B\left(V_i \cos\theta_i\right) \end{aligned} \tag{13}$$

Thus the calculated current phasor quantities I_{ik} and δ_{ik} are functions of the voltage states and π-model line parameters R, X, and B.

For transformers, we use (10)–(13) with some modifications, namely setting $B = 0$ and including the tap ratio by taking into account that current phasors at each end of a transformer are related by

$$\tilde{I}_{Tik} = -a\tilde{I}_{Tki} \tag{14}$$

Thus we have the different equations for each side,

$$\tilde{I}_{Tik} = \frac{1}{R_T + jX_T}\left(\tilde{V}_i - \frac{1}{a}\tilde{V}_k\right) \tag{15}$$

$$\tilde{I}_{Tki} = \frac{1}{R_T + jX_T}\left(\frac{1}{a^2}\tilde{V}_k - \frac{1}{a}\tilde{V}_i\right) \tag{16}$$

where a is the transformer tap ratio and (R_T, X_T) are the transformer series parameters. For simplicity, we assume a is continuous and real (no phase-shifting).

Gauss-Newton Solution Method

We employ the Gauss-Newton iterative method [23] to the solve the phasor state estimation problem for a single time-aligned sample of phasor measurements. When no previous solution is available, we initialize the iteration using a linear state estimator, omitting bias and scaling factors [24].

In our formulation, we take the augmented state vector approach to estimate phase angle biases, current scaling factors, line parameters, and transformer tap ratios.

We assemble the residual equations given by (6)-(9) into vectors e_V, e_θ, e_I, and e_δ, and denote the residual error vector e, state vector x, and augmented parameter vector α as

$$e = \begin{bmatrix} e_V \\ e_\theta \\ e_I \\ e_\delta \end{bmatrix}, \qquad x = \begin{bmatrix} V \\ \theta \end{bmatrix}, \qquad \alpha = \begin{bmatrix} \phi \\ c \\ X \\ B \\ a \end{bmatrix} \tag{17}$$

At each iteration, we update the states and parameters by solving for the increment given by the weighted least-squares problem

$$WH\begin{bmatrix} \Delta x \\ \Delta\alpha \end{bmatrix} = We \tag{18}$$

where H is the measurement Jacobian matrix and W is a diagonal matrix consisting of all weights W_i.

To compute H, we take the partial derivatives of the residual equations with respect to the states and parameters to obtain

$$\begin{aligned} H &= \left[\begin{array}{c|c} \frac{\partial e}{\partial x} & \frac{\partial e}{\partial \alpha} \end{array}\right] \\ &= \left[\begin{array}{cc|ccccc} \frac{\partial e_V}{\partial V} & 0 & 0 & 0 & 0 & 0 & 0 \\ 0 & \frac{\partial e_\theta}{\partial \theta} & \frac{\partial e_\theta}{\partial \phi} & 0 & 0 & 0 & 0 \\ \frac{\partial e_{I_{ik}}}{\partial V} & \frac{\partial e_{I_{ik}}}{\partial \theta} & 0 & \frac{\partial e_{I_{ik}}}{\partial c} & \frac{\partial e_{I_{ik}}}{\partial X} & \frac{\partial e_{I_{ik}}}{\partial B} & \frac{\partial e_{I_{ik}}}{\partial a} \\ \frac{\partial e_{\delta_{ik}}}{\partial V} & \frac{\partial e_{\delta_{ik}}}{\partial \theta} & \frac{\partial e_{\delta_{ik}}}{\partial \phi} & 0 & \frac{\partial e_{\delta_{ik}}}{\partial X} & \frac{\partial e_{\delta_{ik}}}{\partial B} & \frac{\partial e_{\delta_{ik}}}{\partial a} \end{array}\right] \end{aligned} \tag{19}$$

Rank Conditions

For the PSE to have a unique solution, the measurement Jacobian H has to have full rank. Thus it is necessary that

$$2N_V + 2N_I \geq 2N_B + N_\alpha \tag{20}$$

where N_V and N_I are the number of unique voltage and current phasors, N_B is the number of buses, and N_α is the total number of estimated parameters, including angle biases, current scaling factors, tap ratios, and line parameters.

The following are additional rank conditions required for estimating various correction factors and parameters.

Phase Angle Bias Because the phase angle bias depends on angular differences among different bus voltage phasors, we set one PMU as the reference, so its angle bias term is equal to zero ($\phi_{\text{ref}} = 0$). To satisfy the rank condition of H, we require at minimum one current phasor measurement connecting the PMU to the rest of the network.

Current Scaling Estimating a current scaling factor requires redundancy of the current magnitude. Compared to the conditions for angle bias estimation, this condition is more strict, thus we do not estimate scaling factors for every current channel.

Line Parameters and Transformer Tap Ratios Only one current phasor measurement is required to calculate the transmission line parameters (X, B) or transformer parameters (X, a). The voltage phasors at the ends of the line do not need to be directly measured as long as (20) is satisfied.

Application to Central NY Power System

We apply the phasor state estimator to five disturbance events to test the angle bias, current scaling factors, and line parameter estimation under various conditions. We also demonstrate the use of the PSE to monitor power transfer interfaces. Table I provides a list of the events.

TABLE I
RECENT DISTURBANCE EVENTS

Name	Description
Event 1	Loss-of-generation to the East (500 MW)
Event 2	Loss-of-generation to the East (800 MW)
Event 3	Loss-of-generation to the East (700 MW)
Event 4	Loss-of-generation to the West (800 MW)
Event 5	Loss-of-generation to the East (No PMU data from Bus 5)
Event 6	Tap changing (to demonstrate tap ratio estimation)

In Events 1-4, all of the PMUs were reporting data but in Event 5, PMU 5 was not providing data. For each event, we run the PSE at 30 samples per second for a 20-second window of data that includes the disturbance, using the line parameters from the SE model. We choose the data windows such that the disturbances occur between $t = 2$ and $t = 3$ seconds.

Data Quality and Parameter Consistency Analysis

For Events 1-4, we estimate the parameters listed in Table II. In Event 5, the loss of redundancy reduces the number of parameters we can estimate, so we do not estimate the parameters for Line 4–5 (X_{45}, B_{45}) and the angle bias ϕ_5 at Bus 5 is no longer meaningful to estimate.

TABLE II
PARAMETERS

Name	Description
$\phi_{\text{ref}} = 0$	PMU 1A (at Bus 1) is the reference for angle bias
ϕ_1	Angle bias for PMU 1B (at Bus 1)
ϕ_4	Angle bias for PMU 4 (at Bus 4)
ϕ_5	Angle bias for PMU 5 (at Bus 5)
ϕ_{10}	Angle bias for PMU 10 (at Bus 10)
ϕ_{11}	Angle bias for PMU 11 (covers Buses 11 and 12)
c_{46}	Scaling correction for current measurement I_{46}
c_{45}	Scaling correction for current measurement I_{45}
X_{45}	Series reactance for Line 4–5
B_{45}	Shunt susceptance for Line 4–5
$a_{1-10,1}$	Transformer tap ratio on Branch 1–10, Circuit 1
$a_{1-10,2}$	Transformer tap ratio on Branch 1–10, Circuit 2
a_{11-12}	Transformer tap ratio on Branch 11–12

In Figure 5, we plot the scaling factors for two current measurements, I_{46} and I_{45}. The results show a 8-12% error for I_{46} and consistent 7% for I_{45}. Aside from transients during the disturbances, the scaling factors remain relatively constant,

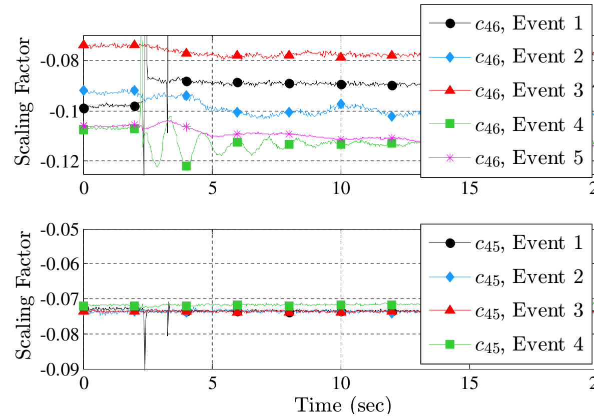

Fig. 5. Scaling Factors for Currents I_{46} & I_{45}

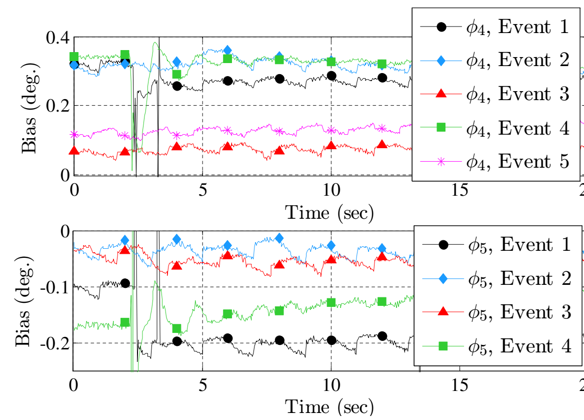

Fig. 6. Angle Bias for PMUs 4 & 5

which can indicate a systematic scaling problem for these two current measurements. Such scaling problems can be readily corrected by adjusting values in the PMU configuration file.

For Events 1-4, we estimate the line parameters on Line 4–5 and compare them to the values from the SE model. We find a 10-15% difference between the nominal and estimated values, which may be due to the fact that Line 4–5 is not transposed.

We observe that for all PMUs, the estimated angle bias is quite small, less than 0.5°. Figure 6 shows the angle bias estimation for PMUs 4 and 5.

Detection of a Timing Signal Problem In the angle bias estimation, we observe a small-amplitude variation (about 0.03°) with periodic, sawtooth-like behavior. Its presence in all of the angle bias variables indicates that the problem is with the reference (PMU 1A). Note that the angle variation is quite small.

Closer examination reveals a period of 2 seconds with transients at the top of each second, which is consistent with a GPS clock pulse. Figure 7 shows the angle bias of PMU 1B and we can see that this problem was resolved by fixing the timing signal circuitry.

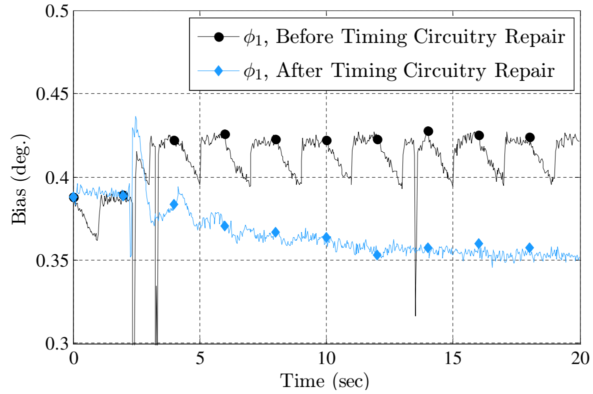

Fig. 7. Angle Bias before/after Timing Circuit Repair

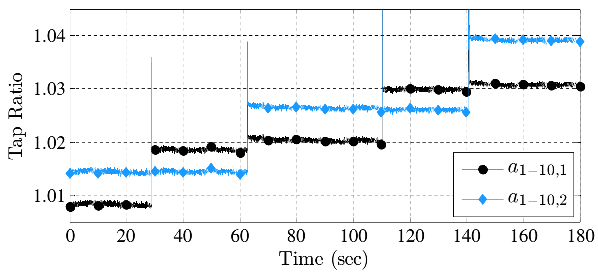

Fig. 8. Transformer Tap Ratio Estimation

Missing PMU Data During Event 5, the data from the PMU at Bus 5 was not being reported, which means we cannot calculate Bus 9, Interface E, or line parameters and scaling factors on Line 4–5. Despite the data loss, we can still estimate the current scaling error on Line 4–6 and all of the results are consistent with the other events (Fig. 5).

Transformer Tap Ratio Estimation We employ the voltage and current phasor measurements at Buses 1 and 10 to estimate the tap ratio of the transformers, which are made by different manufacturers and have different tap ranges and numbers of steps. The tap ratio was found to be constant for Events 1-5, but in a separate dataset (Event 6), the PSE indicated several tap changes. Figure 8 shows the tap ratios for both transformers, indicating four tap changes (two for each transformer). Note that the tap functions are slightly nonlinear, as the tap change in Transformer 2 causes the tap estimate of Transformer 1 to change by about 0.1 %.

Data Quality Improvement

To demonstrate the improvement in data quality, we compare the residual error with and without correction of angle bias in Table III. The RMS error is calculated separately for each group of measurements: voltage magnitude, voltage angle, current magnitude, and current angle. Within each group of measurements, we also list the maximum error. The values in Table III are averaged over the entire 20-second dataset for each event. In all cases the error is decreased when the angle bias is included, but we only include Events 2 and 4 here for brevity. Note that the current scaling factors are used in both the uncorrected and corrected PSE solutions.

TABLE III
RESIDUAL ERROR FOR MULTIPLE EVENTS

Residual error	**Current scaling correction only**		**Current scaling and angle bias correction**	
	RMS	Max	RMS	Max
e_V (Event 2)	0.0146	0.0236	0.0126	0.0207
e_I (Event 2)	0.0939	0.2397	0.0764	0.1563
e_θ (Event 2)	0.1025	0.2209	0.0913	0.1873
e_δ (Event 2)	0.1201	0.2819	0.0817	0.1890
e_V (Event 4)	0.0138	0.0230	0.0121	0.0204
e_I (Event 4)	0.1152	0.2860	0.0904	0.1910
e_θ (Event 4)	0.1097	0.2335	0.0755	0.1411
e_δ (Event 4)	0.1004	0.2341	0.0653	0.1418

As a further demonstration of data quality improvement, we show that the standard deviation of the errors is significantly decreased when bias correction and scaling factors are used. Table IV lists the average standard deviation of the residuals with and without angle bias correction. The results show that the outliers in the data are brought in line with the rest of the data and the PSE solution is more consistent.

TABLE IV
STANDARD DEVIATION OF PSE RESIDUAL ERROR

Residual error	**Current scaling correction only**	**Current scaling and angle bias correction**
	Std. dev. σ	Std. dev. σ
e_V (Event 2)	7.3123×10^{-3}	5.9782×10^{-3}
e_I (Event 2)	8.3864×10^{-2}	6.9853×10^{-2}
e_θ (Event 2)	1.3550×10^{-3}	1.2591×10^{-3}
e_δ (Event 2)	1.7974×10^{-3}	1.2357×10^{-3}
e_V (Event 4)	6.5456×10^{-3}	5.6627×10^{-3}
e_I (Event 4)	10.202×10^{-2}	8.1418×10^{-2}
e_θ (Event 4)	14.676×10^{-4}	9.8815×10^{-4}
e_δ (Event 4)	14.275×10^{-4}	9.3691×10^{-4}

In Table V, we show a decrease in total vector error (TVE) when angle bias correction is used. Here we treat the PSE solution as the exact solution and compare it to the measurements. The values in Table V are averaged across all PMUs and over the 20-second window for each disturbance event.

Interface Flows for Disturbance Events

After the phasor state estimation is completed, we can compute the interface flows for the observable network. We look at two

TABLE V
MEAN TOTAL VECTOR ERROR (TVE)

Event	**Current scaling correction only**	**Current scaling and angle bias correction**
	Mean TVE	Mean TVE
Event 1	1.162%	0.890%
Event 2	1.106%	0.907%
Event 3	0.993%	0.701%
Event 4	1.051%	0.852%

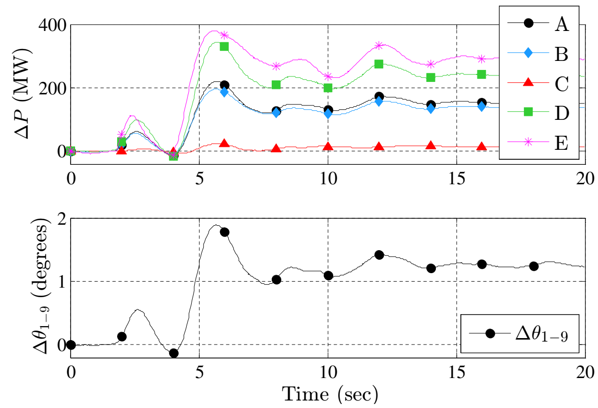

Fig. 9. Interface Flows and Angle Separation, Event 2

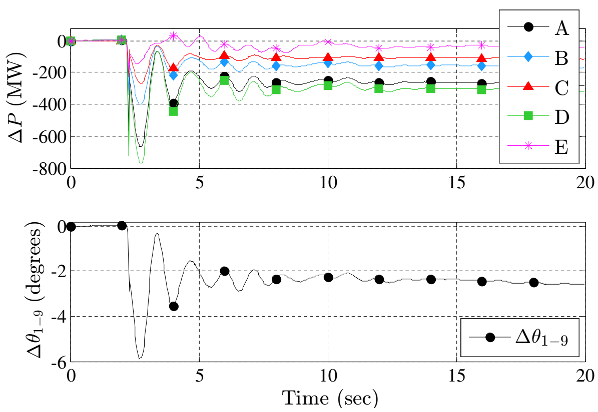

Fig. 10. Interface Flows and Angle Separation, Event 4

loss-of-generation events (Events 2 and 4).

Event 2: Loss of Generation to the East Event 2 is a loss-of-generation event occurring in the external system beyond Bus 2. The power system responds by increasing the power flows across Interfaces A, B, D, and E. Figure 9 shows the net change in interface power flow and angle separation between Bus 1 and Bus 9 for this event.

There is little change in flow across the North-South Interface C but on the other hand, there is a 250-300 MW increase in active power across Interface E, representing about one-third of the generation lost. We also observe an increase in the angle separation that settles around 1.2° from its original value.

Event 4: Loss of Generation to the West In Event 4, we see a net decrease in flow across the interface because power is lost to the west. The net decrease in flow is due to the fact that power flow is normally in the opposite direction. The change in interface flows and angle separation is shown in Figure 10. We see that 300 MW of the 800 MW lost is supplied from the East (across Interface D) and the flow decrease across Interface E is quite small. The angle separation between Buses 1 and 9 rapidly decreases by 6°, but settles around 2.5° lower than the original value.

With these two loss-of-generation events, we demonstrate the utility of the PSE method for computing unmeasured line flows and constructing a high-fidelity picture of the transmission system, enabling wide-area system monitoring and control using PMUs.

Oscillation Mode Damping

The oscillation mode damping using PMU measurement has been discussed in several papers [25]–[27]. The current structure of power system controllers aiming at damping electromechanical oscillations is decentralized. Power system stabilizers (PSSs) use local signals and their outputs act on the excitation system of the synchronous generators. Power system stabilizers are tuned to be effective on local and interarea modes in a range of system conditions. Although the current control structure tends to be robust and very effective, requirements of optimization and robustness in the PSSs design would be desirable, given the current constraints in transmission system expansion, leading to a more intensive use of the existing transmission assets and to lower stability margins. However, a comprehensive design of all controllers in a large system could face several problems because it involves the need of retuning PSSs in several utilities and the selection of parameters to achieve not only local but also the global performance requirements. Besides, changes in the system configuration as new lines and interconnections are put into operation may require global retuning of PSSs as new oscillation modes emerge.

Hierarchical control structures using the facilities provided by phasor measurements could add to the existing solutions for the problems discussed above. Hierarchical control structures were proposed in [27]–[31]. In this work a hierarchical control scheme with two-levels, a decentralized control structure and a centralized control structure, is utilized. The former uses a decentralized structure, acting locally at the excitation system. This is the conventional decentralized control structure found in the power industry. The later is a higher level centralized controller. This is quite different from the current control structures used in the industry, but with the development of phasor measurements and communication facilities it can be considered as a serious possibility in the control of future power systems. The basic control structure is presented in Figure 11.

Decentralized control structure

This is the conventional decentralized control structure used in the power industry. In this case local controllers, the PSSs, act on the excitation system in each plant. The local structure ensures a minimum performance of the system, even in the event of loss of communication links or a failure that makes the central control unavailable, and the stabilizing action for local modes for which global information may not be necessary.

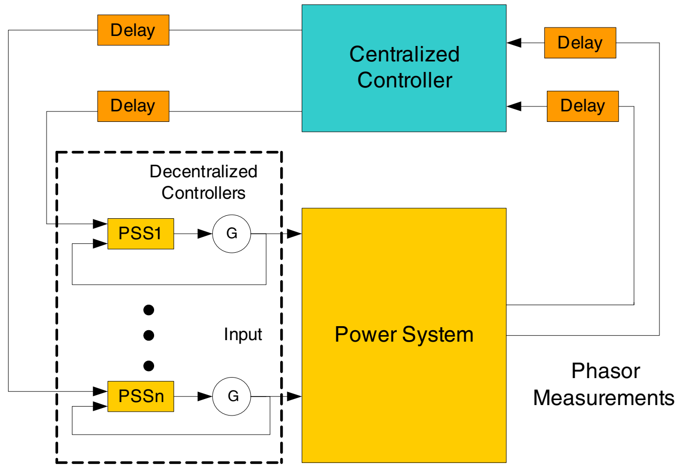

Fig. 11. Two-level control structure

Centralized controller

The centralized structure consists of a central controller and allows the optimization of the global performance of the system. The input could use all the available information acquired by the phasor measurement system. The output is transmitted to the excitation system of the plants that are under this central control. In this work it is assumed that the function of the central controller is performed by the PDC (Phasor Data Concentrator).

The centralized controller can perform several functions besides the optimization of the performance as measured by higher damping levels of the oscillation modes. Robustness requirements can be included in the design of the central controller to take into account changes in the system topology and large variations in load and power flows. Currently, taking robustness as a requirement faces difficulties of implementation because it requires retuning of PSSs in several utilities with global goals that may not be so clear for the utilities, or implementing new techniques, such as adaptive control, that are not well-tested for power systems applications. Supplementary damping sources such as FACTS devices, currently used for other goals as voltage control and power flow control, could additionally be used by the centralized control for optimization and robustness purposes.

The remote signal generated by the central control acts at the excitation system as shown in Figure 12.

Because the remote control signal is calculated in the PDC acting as a central controller, there are two time delays involved, one from the signal measurement point to the PDC and one from the PDC to the power plant, as shown in Figure 11

Design of power systems damping controllers

The controllers for enhancing power systems small-signal stability use output feedback, because the large dimension

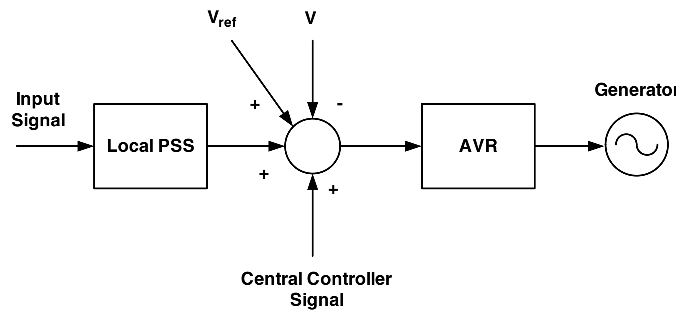

Fig. 12. Actuation of central control signal

turns difficult to use state feedback.

However, the design of output feedback controllers is still an open problem in control theory [32]. It is recognized as a difficult problem, specially in the case in which the controller order is much lower than the controlled system. The inclusion of robustness requirements makes the problem even more difficult. Many publications tackle this problem, but power system engineers have had difficulties in applying these results to real systems.

A considerable range of control design methods applied to power systems are based on optimization. The quadratic regulator problem (LQG) has been applied in several variants to power systems. The performance index is a functional and the minimization is achieved by a solution of a Riccati equation [27]. However, it has a non-explicit relation with the closed-loop performance indexes and does not include robustness requirements

Optimization of objective functions that incorporate closed-loop performance indexes has been proposed for the design of power system controllers [33]–[36]. The success of this approach depends on the nature of the optimization problem. If the performance index leads to a nonsmooth, nonconvex objective function, the optimization method must be able to deal with those characteristics. That is the case of the algorithm used in [37]. It uses a hybrid algorithm mixing quasi-Newton BFGS, bundling and gradient sampling. Its advantage is its capability in handling nonsmooth, nonconvex optimization problems. This allows that performance indexes directly related to the closed-loop performance, but leading to nonsmooth and nonconvex optimization problems, be optimized. A different algorithm is used in [**?**], where a direct search method that can deal with nonsmoothness is applied for the design of power system stabilizers. It is worth remarking that metaheuristics has been proposed as an alternative for solving the problem of designing power system controllers by the optimization of closed-loop performance indexes. Such methods include genetic algorithms [38], simulated annealing [39] and swarm optimization [40]. Robustness requirements can be included. A comparative assessment of the performance of both approaches for the design of power system controllers involving nonsmooth and nonconvex functions must yet be carried out.

Damping Improvement The design method proposed in [27] is applied to a 33-bus, seven-machine equivalent model of the Southern Brazil system (Fig. 13). This equivalent was specially prepared to test applications in the Southern Brazil system. The generators are represented by a fifth-order model. Generator saturation is included. Besides AVR and PSS, speed governors are represented. Wash-outs are included in the local and central PSS and all devices are represented considering their limits. The complete system data is found in [27].

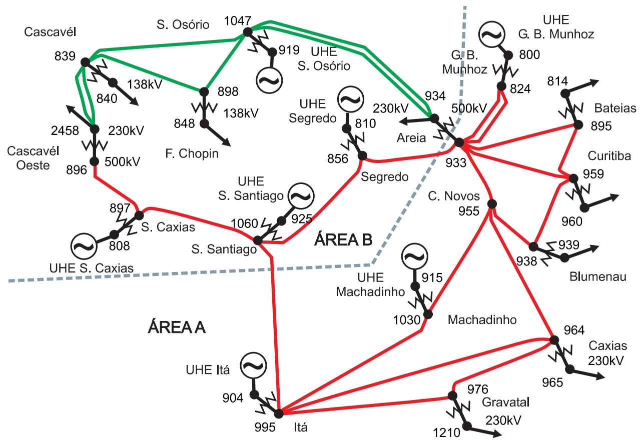

Fig. 13. Equivalent of Southern Brazil system.

The system is originally well-damped with the decentralized control. All modes present damping above 13%. However, under critical topological changes, the system damping can decrease significantly. For instance, the permanent disconnection of the transmission line 995-1060 (Ita-S. Santiago) causes the emergence of a low-damped mode (Table VI, Row 1). This mode is associated to the oscillation of generators Ita and Machadinho against the rest of the system. The system performance can be improved by retuning of the conventional PSSs but this is time consuming and can restrict temporarily the optimal real-time operation. A two-level control can be promptly enabled from the EMS in order to ensure a high damping for the new topology and is an alternative to the retuning of the PSSs in several utilities.

TABLE VI

TEST SYSTEM DOMINANT OSCILLATION MODES

Case	Row Number	Eigenvalue	Frequency (Hz)	Damping (%)
Local control	1	$-0.12 \pm 4.92i$	0.78	2.53
Two-level control	2	$-0.57 \pm 6.42i$	1.02	8.86

Controller design

The synthesis of the central controller can be cast as an optimization problem. A H_∞ norm minimization is applied between the voltage reference and the angle speed, this time at the Machadinho power plant. The central controller was designed using as input signals the generator speeds of Salto Caxias, Ita, Salto Osorio and Machadinho with outputs at the same power plants. The selection of input and outputs was based on the analysis of the controllability and observability factors corresponding to the low-damped mode. Time delays of 200 ms, between the PMUs and the PDC, and from the PDC to the generators under the central controller, in a total of 400 ms, were considered. The system order, including time delays, was chosen. The computing time for the Southern system is in the order of seconds, a much shorter time than in the case of the Southern/Southeastern system. The improved system damping with the two-level control is shown in Table VI, Row 2.

Conclusions

In this paper, three main components related with the phasor measurement research were discussed, contributing to improve the power system operation performance. First, it necessary to have a better understanding of the way the phasor is measured in off-line analysis. Second, the PMU like any other device may present measurement errors during regular operation and needs to be corrected to provide a trustable data for the applications. Third, an advanced application is considered showing the potential of the technology in improving power system operation.

References

[1] A. G. Phadke and B. Kasztenny, "Synchronized phasor and frequency measurement under transient conditions," *IEEE Trans. Power Del.*, vol. 24, no. 1, pp. 89–95, 2009.

[2] A. G. Phadke and J. S. Thorp, *Synchronized phasor measurements and their applications*. New York: Springer, 2008.

[3] M. Akke and J. S. Thorp, "Sample value adjustment improves phasor estimation at off-nominal frequencies," *IEEE Trans. on Power Delivery*, vol. 25, no. 4, pp. 2255–2263, 2010.

[4] M. Paolone, A. Borghetti, and C. A. Nucci, "A synchrophasor estimation algorithm for the monitoring of active distribution newtorks in steady state and transient conditions," in *Proc. 17th Power systems Computation Conference*, 2011.

[5] T. Nguyen and X. Li, "A fast and accurate method for estimating power systems phasors using DFT with interpolation," in *IEEE PES General Meeting*, 2006, p. 8 pp.

[6] W. Premerlani, B. Kasztenny, and M. Adamiak, "Development and implementation of a synchrophasor estimator capable of measurements under dynamic conditions," *Power Delivery, IEEE Transactions on*, vol. 23, no. 1, pp. 109 –123, jan. 2008.

[7] J. dela O. Serna, "Dynamic phasor estimates for power system oscillations and transient detection," in *Power Engineering Society General Meeting, 2006. IEEE*, 2006, p. 7 pp.

[8] G. Benmouyal, "Design of a combined digital global differential and volt/hertz relay for step-up transformers," *IEEE Trans. Power Del.*, vol. 6, no. 3, pp. 1000–1007, 1991.

[9] G. C. Zweigle, L. S. Anderson, and A. Guzman-Casillas, "Tapparatus and algorithm for estimating synchronized phasors at pre-determined times referenced to an absolute time standard in an electrical system," US Patent 7 480 580, 2009.

[10] L. R. S. Anderson, A. Guzman-Casillas, G. C. Zweigle, and G. Ben, "Protective relay with synchronized phasor at pre-determined time referencedto an absolute time standard in an electrical sys," US Patent 6 845 333, 2005.

[11] D. Dotta and J. Chow, "Second harmonic filtering in phasor measurement estimation," *Power Delivery, IEEE Transactions on*, vol. 28, no. 2, pp. 1240–1241, 2013.

[12] D. W. P. Thomas and M. S. Woolfson, "Evaluation of frequency tracking methods," *IEEE Trans. on Power Delivery*, vol. 16, no. 3, pp. 367–371, 2001.

[13] M. M. Begovic, P. M. Djuric, S. Dunlap, and A. G. Phadke, "Frequency tracking in power networks in the presence of harmonics," *IEEE Trans. Power Del.*, vol. 8, no. 2, pp. 480–486, 1993.

[14] M. Akke, “Frequency estimation by demodulation of two complex signals,” *IEEE Trans. Power Del.*, vol. 12, no. 1, pp. 157–163, 1997.

[15] I. Kamwa, M. Leclerc, and D. McNabb, “Performance of demodulation-based frequency measurement algorithms used in typical pmus,” *IEEE Trans. Power Del.*, vol. 19, no. 2, pp. 505–514, 2004.

[16] D. Fan and V. Centeno, “Phasor-based synchronized frequency measurement in power systems,” *IEEE Trans. Power Del.*, vol. 22, no. 4, pp. 2010–2016, 2007.

[17] ——, “Least-squares estimation in phasor-based synchronized frequency measurements,” in *Proc. IEEE Power and Energy Society General Meeting - Conversion and Delivery of Electrical Energy in the 21st Century*, 2008, pp. 1–6.

[18] T. S. J. Warichet and J. C. Maun, “Considerations about synchrophasors measurement in dymanic system conditions,” *Electrical Power and Energy Systems*, vol. 31, no. 9, pp. 452–464, October 2009.

[19] M. M. Giray and M. S. Sachdev, “Off-nominal frequency measurements in electric power systems,” *IEEE Trans. Power Del.*, vol. 4, no. 3, pp. 1573–1578, 1989.

[20] A. A. Girgis and T. L. D. Hwang, “Optimal estimation of voltage phasors and frequency deviation using linear and nonlinear Kalman filtering: Theory and limitations,” *IEEE Power Eng. Rev.*, no. 10, pp. 46–47, 1984.

[21] L. Vanfretti, J. H. Chow, S. Sarawgi, and B. Fardanesh, “A phasor-data-based state estimator incorporating phase bias correction,” *IEEE Trans. Power Syst.*, vol. 26, no. 1, pp. 111–119, 2011.

[22] A. Abur and A. G. Expósito, *Power System State Estimation: Theory and Implementation*. New York: Marcel Dekker, 2004.

[23] Å. Björck, *Numerical Methods for Least Squares Problems*. Philadelphia, PA: Society for Industrial and Applied Mathematics, 1996.

[24] A. G. Phadke and J. S. Thorp, *Synchronized Phasor Measurements and Their Applications*. New York: Springer, 2008.

[25] J. H. Chow, J. J. Sanchez-Gasca, H. Ren, and S. Wang, “Power system damping controller design-using multiple input signals,” *IEEE Control Systems*, vol. 20, no. 4, pp. 82–90, 2000.

[26] D. Dotta, A. S. e Silva, and I. C. Decker, “Design of power system controllers by nonsmooth, nonconvex optimization,” in *Proc. IEEE Power & Energy Society General Meeting PES ’09*, 2009, pp. 1–7.

[27] ——, “Wide-area measurements-based two-level control design considering signal transmission delay,” *IEEE Transaction on Power System*, vol. 24, no. 1, pp. 208–216, 2009.

[28] I. Kamwa, R. Grondin, and Y. Hï£¡bert, “Wide-area measurement based stabilizing control of large power sytems - a decentralized/hirarchical approach,” *IEEE Transactions on Power Systems*, vol. 16, no. 1, pp. 136–153, February 2001.

[29] H. Ni, G. T. Heydt, and L. Mili, “Power system stability agents using robust wide-area control,” *IEEE Trans. on Power Systems*, vol. 17, no. 4, pp. 1123–1131, november 2002.

[30] F. A. Okou *et al.*, “Large power system stability enhancement using wide-area signals based hierarchical controller,” in *Proc. IEEE PES General Meeting*, Denver, 2004.

[31] ——, “Smith prediction approach for the design of a robust wide-area measurements based hierarchical controller,” in *Proc. IEEE PES General Meeting*, San Francisco, 2005.

[32] V. D. Blondel, M. Gevers, and A. Lindquist, “Survey on the state of systems and control.” *European Journal of Control*, vol. 5-23, p. European Journal of Control, 1995.

[33] C. D. Vournas and B. C. Papadias, “Power system stabilization via parameter optimization - application to the hellenic interconnected system,” *IEEE Trans. Power Syst.*, vol. 2, no. 3, pp. 615–622, 1987.

[34] M. Khaldi, A. Sarkar, K. Lee, and Y. Park, “The modal performance measure for parameter optimization of power system stabilizers,” *IEEE Trans. Energy Convers.*, vol. 8, no. 4, pp. 660–666, 1993.

[35] Y.-Y. Hong and W.-C. Wu, “A new approach using optimization for tuning parameters of power system stabilizers,” *IEEE Trans. Energy Convers.*, vol. 14, no. 3, pp. 780–786, 1999.

[36] I. Kamwa, G. Trudel, and L. Gerin-Lajoie, “Robust design and coordination of multiple damping controllers using nonlinear constrained optimization,” in *Power Industry Computer Applications, 1999. PICA ’99. Proceedings of the 21st 1999 IEEE International Conference*, 1999, pp. 87–94.

[37] J. V. Burke, A. S. Lewis, and M. L. Overton., “Hifoo - a matlab package for fixed-order controller design and h-infinity optimization,” in *Fifth IFAC Symposium on Robust Control Design*, 2006.

[38] A. L. Bomfim, G. Taranto, and D. Falcao, “Simultaneous tuning of power system damping controllers using genetic algorithms,” *IEEE Trans. Power Syst.*, vol. 15, no. 1, pp. 163–169, 2000.

[39] M. Abido, “Robust design of multimachine power system stabilizers using simulated annealing,” *IEEE Trans. Energy Convers.*, vol. 15, no. 3, pp. 297–304, 2000.

[40] ——, “Optimal design of power-system stabilizers using particle swarm optimization,” *IEEE Trans. Energy Convers.*, vol. 17, no. 3, pp. 406–413, 2002.